Available online at www.sciencedirect.com
SCIENCE DIRECT®
Journal of Nuclear Materials 329–333 (2004) 597–601
journal of nuclear materials
www.elsevier.com/locate/jnucmat

Calculation of radiation-induced deformation of SUS 316 in the ITER-relevant condition

Johsei Nagakawa [a,b,*], Keiko Ueno [a,b]

[a] *Advanced Nuclear Materials Group, National Institute for Materials Science (NIMS), 1-2-1 Sengen, Tsukuba, Ibaraki 305-0047, Japan*
[b] *Interdisciplinary Graduate School of Engineering Sciences, Kyushu University, 6-1 Kasuga Koen, Kasuga, Fukuoka 816-8580, Japan*

Abstract

SUS 316 stainless steel will be used in ITER as a major structural material. However, accumulation of radiation-induced deformation data in the anticipated operation temperature range, centered at about 300 °C, is not adequate. Although it will be used mainly in annealed condition, cold-working and consequent introduction of network dislocations is inevitable at various parts of the structure. Computer simulation was performed to examine the radiation-induced deformation of SUS 316 steel, with emphasis on the effect of network dislocation density, for the ITER-relevant condition. Irradiation creep rates and radiation-induced stress relaxation behaviors were examined at 300 °C for various displacement rates, applied stresses and network dislocation densities. Rather complicated dependence on dislocation density has been predicted in both creep deformation and stress relaxation. This complexity results from a competitive redistribution of point defects to the operating deformation mechanisms and from the predominance among them that depends on the network dislocation density.

1. Introduction

SUS 316 stainless steel will be used in ITER as a major structural material for blankets and vacuum vessels. However, the accumulation of radiation-induced deformation (irradiation creep and radiation-induced stress relaxation) data in the anticipated temperature range, centered at about 300 °C, is not sufficient. Particularly, the dislocation density dependence has not been examined adequately, despite the fact that cold-working and consequent introduction of network dislocations is possible in various parts of the ITER structure, although the material will be used mainly in annealed condition.

Recently, cracks have been found in the core structures, particularly the shrouds, of many light water cooled reactors in Japan. One of the key factors for the initiation of these cracks is suspected to be a tensile residual stress at the surface layer introduced by the final grinding and polishing, especially in the vicinity of weld joints. Radiation-induced deformation, especially leading to stress relaxation, may influence such cracking of the reactor core structure by reducing the residual stress [1] or by affecting the crack propagation process [2]. This indicates the importance of the dislocation density dependence of the radiation-induced deformation in ITER as well as in light water reactors.

In the present study, computer simulation was performed to examine the radiation-induced deformation of SUS 316 steel at 300 °C, with emphasis on the effects of network dislocation density. Some of the results on dislocation density dependence were compared with the

* Corresponding author. Address: Advanced Nuclear Materials Group, National Institute for Materials Science (NIMS), 1-2-1 Sengen, Tsukuba, Ibaraki 305-0047, Japan. Tel.: +81-29 859 2553/2014; fax: +81-29 859 2014.
E-mail address: nagakawa.johsei@nims.go.jp (J. Nagakawa).

0022-3115/$ - see front matter © 2004 Elsevier B.V. All rights reserved.
doi:10.1016/j.jnucmat.2004.04.106

experimental results obtained using light ion irradiation and published in a separate report [3].

2. Modeling and calculation procedure

The calculation is based on the stress-influenced kinetics of nucleation and growth of defect agglomerates, as well as point defect absorption by network dislocations [4]. Simultaneous differential equations are numerically solved for the following defect concentrations: (1) single interstitials (C_i), (2) single vacancies (C_v), (3) aligned interstitial loop precursors (C_{2iA}), (4) non-aligned interstitial loop precursors (C_{2iN}), (5) growing interstitial loops on aligned planes (C_{ilA}), (6) those on non-aligned planes (C_{ilN}), (7) accumulated net interstitials in growing aligned loops (C_{ilAi}), (8) those in growing non-aligned loops (C_{ilNi}), (9) net interstitials absorbed by aligned network dislocations (C_{dAi}), (10) those absorbed by non-aligned network dislocations (C_{dNi}).

Migration energies of point defects were adopted from the evaluation provided by Dimitrov and Dimitrov [5]. Important parameter values used in the numerical calculation are listed in Table 1. Z_i (interstitial bias) and ΔZ_i (stress-induced bias) for loops and network dislocations were calculated using the equations given by Wolfer and Ashkin [6] and Heald and Speight [7], respectively. At each numerical iteration step the loop size was re-averaged, and $Z_{i,v}$ and $\Delta Z_{i,v}$ were re-evaluated. In the interstitial loop nucleation process, the di-interstitial was assumed to be the precursor and the formation of loops was considered to be under the influence of external stress, following the SIPN model proposed by Brailsford and Bullough [8].

Table 1
Parameter values used in this calculation

Parameter	Value
Defect migration energy	
Interstitial	0.92 eV
Vacancy	1.15 eV
Defect migration pre-exponent	
Interstitial	8.0×10^{-7} m^2/s
Vacancy	1.4×10^{-6} m^2/s
Lattice constant	3.524×10^{-10} m
Atomic volume	1.1×10^{-29} m^3
Strength of Burgers vector	2.16×10^{-10} m
Young's modulus	2.6×10^{5} MPa
Shear modulus	1.0×10^{5} MPa
Poisson's ratio	0.3
Defect relaxation volume	
Interstitial	+1.4 × atomic volume
Vacancy	−0.46 × atomic volume
Difference in shear modulus	
Between defect and matrix	
Interstitial	-1.0×10^{5} MPa
Vacancy	0 MPa

In the present study, SIPN (stress-induced preferential nucleation of interstitial loops) [8,9] and loop growth driven by SIPA (stress-induced preferred absorption of point defects) [7,10] are taken into account, as well as PA (SIPA climb) and PAG (glide enabled by SIPA climb) contributions [11] by network dislocations. From the calculated derivatives of defect concentrations, the plastic strain rate produced by each mechanism was evaluated at every iteration step using the following equations. This approach is quite different from the analytical calculation based on each single mechanism.

(1) PA (SIPA climb creep by network dislocations) [11],

$$\dot{\varepsilon}_{PA} = \frac{2}{3}(dC_{dAi}/dt - dC_{dNi}/dt), \tag{1}$$

(2) PAG (dislocation glide induced by SIPA climb) [11],

$$\dot{\varepsilon}_{PAG} = (4e\sqrt{\pi L_d}/3b)(dC_{dAi}/dt - dC_{dNi}/dt), \tag{2}$$

(3) SAIL (SIPA climb creep by growing interstitial loops) [7,10],

$$\dot{\varepsilon}_{SAIL} = \frac{2}{3}(dC_{ilAi}/dt - dC_{ilNi}/dt), \tag{3}$$

(4) SIPN (creep by stress-induced preferential loop nucleation) [8,9],

$$\dot{\varepsilon}_{SIPN} = \frac{4}{3}(dC_{2iA}/dt - dC_{2iN}/dt), \tag{4}$$

where e is the elastic deflection (σ/E; σ is the external stress, E is Young's modulus), L_d is the network dislocation density, and b is the size of the Burgers vector. Such a calculation procedure allows all the deformation mechanisms to operate simultaneously, competing for the point defects, and simulates the dynamic situation under irradiation.

Stress relaxation was also calculated directly by the computer simulation using the same procedure except for a minor change. The amount of stress reduction $\Delta\sigma$ due to the total plastic strain increment $\Delta\varepsilon_p$ produced by all the mechanisms during each iteration step was evaluated using the equation,

$$\frac{d\sigma}{dt} = -E\frac{d\varepsilon_p}{dt} \Rightarrow \Delta\sigma = -E\Delta\varepsilon_p. \tag{5}$$

All kinetic parameters for the next iteration step were recalculated with the reduced stress. This elaborate procedure gives a reliable estimate even when the radiation-induced deformation involves a non-steady state period. This approach has shown good agreement with conventional results obtained using the power law creep rate when there is no significant transient [12].

In the following, a nominal dpa value, not the value multiplied by the damage efficiency, is used to describe the damage and the damage rate. Since the in-reactor creep compliance is generally about 0.3 times that for the light-ion irradiation creep [13], the damage and the damage rate should be multiplied by 0.3 for neutron irradiation.

3. Results and discussion

Fig. 1 shows the stress dependence of irradiation creep rate at 2×10^{-7} dpa/s that corresponds to the displacement rate anticipated at the blanket position of ITER [14]. The examined dislocation density ranges from 3×10^{12} to 3×10^{15} m^{-2}, representing a well annealed and a heavily cold-worked condition, respectively. At all dislocation densities, the stress dependence is almost linear below 100 MPa and gradually increases at higher stresses. However, the stress dependence is still very weak compared with that without irradiation. A stress exponent close to unity leads to significant stress relaxation, because considerable plastic deformation is still produced, which will lead to another large elastic stress reduction, on the contrary to the non-irradiation case in which the stress exponent is as large as 4–6 and the plastic deformation declines to a large extent as the stress is decreased.

The dependence of irradiation rate on dislocation density is calculated for 10, 100 and 500 MPa at 2×10^{-7} dpa/s as shown in Fig. 2. The dependence is not a simple function of dislocation density and it has a maximum around 10^{14} m^{-2} for all stresses examined. When the displacement rate decreases, the shape of the dependence changes, as shown in Fig. 3 for 1×10^{-9} dpa/s which corresponds to the conditions anticipated in the vacuum vessel position in ITER [14]. The minimum creep rate shifts from 4×10^{14} m^{-2} to 2×10^{15} m^{-2}, as the stress level increases.

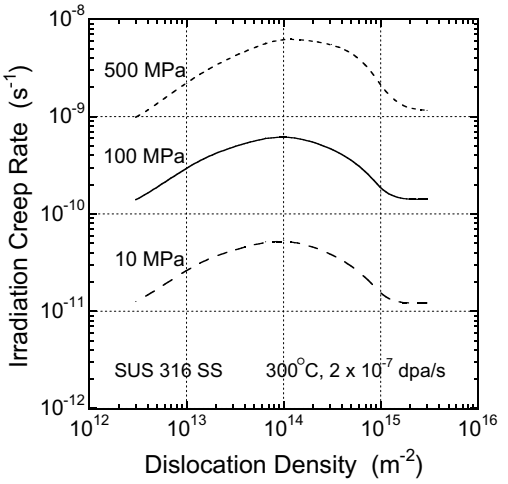

Fig. 2. Dislocation density dependence of irradiation creep rate at 2×10^{-7} dpa/s for 10, 100 and 500 MPa.

Contribution to the dislocation density dependence from each deformation mechanism is shown in Fig. 4. As the dislocation density increases, loss of point defects via bulk recombination decreases and each creep mechanism produces increasing creep deformation. However, the contribution of SIPN diminishes swiftly above 10^{14} m^{-2} where most of the point defects are absorbed by network dislocations, and loop nucleation declines. Fig. 5 shows the same dependence as Fig. 4 but for a much lower displacement rate of 1×10^{-9} dpa/s.

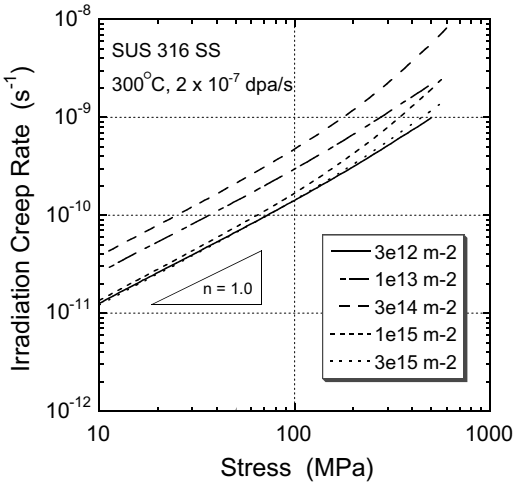

Fig. 1. Stress dependence of irradiation creep rate at 2×10^{-7} dpa/s with various dislocation densities.

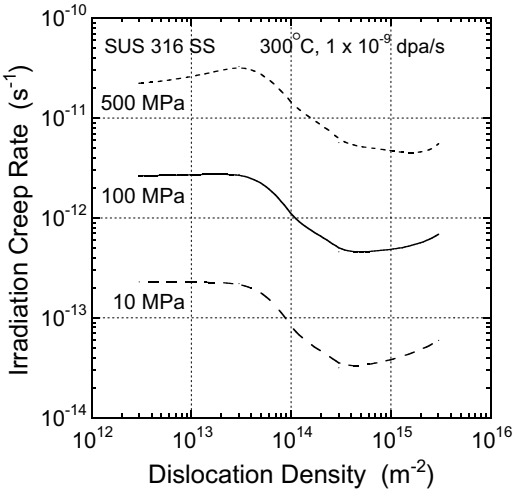

Fig. 3. Dislocation density dependence of irradiation creep rate at 1×10^{-9} dpa/s for 10, 100 and 500 MPa.

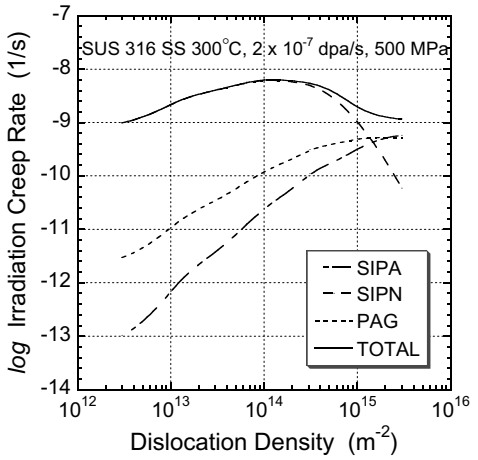

Fig. 4. Creep rate contribution from each mechanism at 2×10^{-7} dpa/s and 500 MPa.

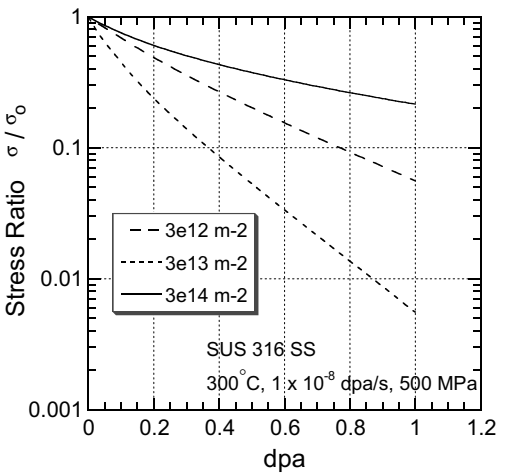

Fig. 6. Stress relaxation at 2×10^{-7} dpa/s for various dislocation densities.

The dependence of each mechanism appears to shift to lower dislocation densities, arising from the smaller bulk recombination rate at this lower damage rate.

Dislocation density influences the radiation-induced creep rate and thereby the stress relaxation, as indicated in Fig. 6 for 1×10^{-8} dpa/s, 500 MPa and three different dislocation densities. Stress relaxes swiftly at 3×10^{13} m^{-2}, but relaxes more slowly at both higher and lower dislocation densities. For a displacement rate of 1×10^{-8} dpa/s, the irradiation creep rate shows a maximum around 10^{13} m^{-2} and goes down with decreasing or increasing dislocation density. The stress relaxation behavior also depends on the displacement rate. For instance, with a network dislocation density of 3×10^{12} m^{-2} at 300 °C and 100 MPa, higher displacement rates at the blanket position lead to a slower relaxation rate, while lower displacement rates at the vacuum vessel position would cause a much faster relaxation rate per dpa.

During the lifetime of ITER, microstructure change is expected. Nucleation and growth of dislocation loops have been included in the present calculation as explained in the procedure section. Another constituent of the microstructure evolution is the change of network dislocation density, but this would not be so significant under the ITER condition, maximum of about 10 dpa at 100–300 °C, as the experimental data indicate [15]. Thus, Fig. 6 shows how the stress relaxation will proceed during the evolution of microstructure in ITER.

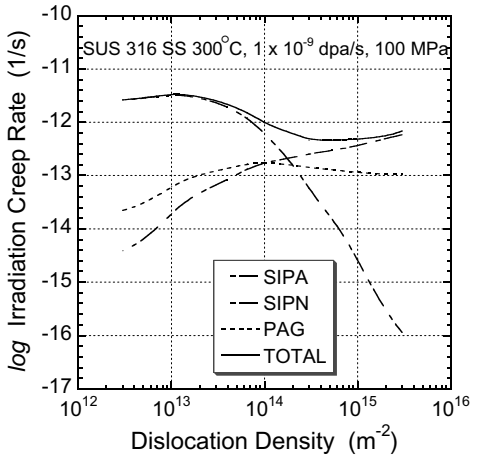

Fig. 5. Creep rate contribution from each mechanism at 1×10^{-9} dpa/s and 100 MPa.

4. Conclusions

Numerical computer calculation was carried out to assess the radiation-induced deformation of SUS 316 stainless steel in the ITER-relevant condition with emphasis on the effect of network dislocation density. The results are summarized as follows.

(1) A rather complicated dependence on dislocation density has been predicted in the radiation-induced deformation behavior. There appears to be both a maximum and/or a minimum in the dislocation density dependencies of creep rate and stress relaxation rate.
(2) This complexity mainly results from a competitive redistribution of point defects, responding to the competing deformation mechanisms, which depends on the network dislocation density.

Acknowledgements

This work was financially supported by the Budget for Nuclear Research of the Ministry of Education, Culture, Sports, Science and Technology, based on the screening and counseling by the Atomic Energy Commission.

References

[1] J. Nagakawa, J. Nucl. Mater. 225 (1995) 1.
[2] J. Nagakawa, Y. Murase, N. Yamamoto, T. Fukuzawa, J. Nucl. Mater. 283–287 (2000) 391.
[3] K. Ueno, J. Nagakawa, Y. Murase, N. Yamamoto, J. Nucl. Mater, these Proceedings, doi:10.1016/j.jnucmat.2004.04.105.
[4] J. Nagakawa, N. Yamamoto, H. Shiraishi, J. Nucl. Mater. 179–181 (1991) 986.
[5] C. Dimitrov, O. Dimitrov, J. Phys. F 14 (1984) 793.
[6] W.G. Wolfer, M. Ashkin, J. Appl. Phys. 46 (1975) 547;
W.G. Wolfer, M. Ashkin, J. Appl. Phys. 46 (1975) 4108.
[7] P.T. Heald, M.V. Speight, Philos. Mag. 29 (1974) 1075.
[8] A.D. Brailsford, R. Bullough, Philos. Mag. 27 (1973) 49.
[9] R.V. Hesketh, Philos. Mag. 7 (1962) 1417.
[10] R. Bullough, J.R. Willis, Philos. Mag. 31 (1975) 855.
[11] L.K. Mansur, Philos. Mag. A 39 (1979) 497.
[12] J. Nagakawa, J. Nucl. Mater. 212–215 (1994) 541.
[13] P. Jung, J. Nucl. Mater. 113 (1983) 133.
[14] Technical Basis for the ITER Final Design, ITER EDA Documentation Series No. 22, IAEA, Vienna, 2001.
[15] P.J. Maziasz, J. Nucl. Mater. 191–194 (1992) 701.